

Molecular Dynamics Simulation of the Interfacial Behavior of Short-Chain Polystyrene Sulfonate Aqueous Solutions in Contact with Graphene Surfaces in the Presence of Multivalent Cations

Ariel A. Chialvo^{*,†} and J. Michael Simonson[‡]

Chemical Sciences Division, Aqueous Chemistry and Geochemistry Group, Oak Ridge National Laboratory, Oak Ridge, Tennessee 37831-6110, Center for Nanophase Materials Sciences Division and Chemical Sciences Division, Macromolecular Structures Group, Oak Ridge National Laboratory, Oak Ridge, Tennessee 37831-6493

Received: May 12, 2008; Revised Manuscript Received: September 25, 2008

We present a detailed analysis of the behavior of aqueous electrolyte–polyelectrolyte systems in contact with neutral and charged graphene substrates, based on an extensive molecular dynamics simulation effort. Our study involves aqueous systems comprising short chains of lithium polystyrene sulfonate with an explicit atomistic description of water, the chain backbones, and their interactions with all species in solution as well as with the graphene surface. We place special emphasis on the behavior of the axial profiles of species concentrations, local electrostatic charge density, electric field, and corresponding surface-charge screening to provide a full characterization of the inhomogeneous environment at the solid–liquid interface, that is, the electric double layer and the effect of the added salts (BaCl_2 and LaCl_3) on its structure. To complete the analysis, we assess the tendency toward ion pairing along planes parallel to the graphene surface and estimate, according to the axial distribution profiles, the strength of the adsorption of the polyelectrolyte, counterions, and other species in solution, in order to interpret the degree of surface-charge screening and the occurrence of surface-charge overcompensation and reversal. We present evidence of a recently reported new phenomenon of overcharging and discuss the central role played by the explicit description of the solvent on this occurrence. Moreover, to interpret the conformational behavior of the polyelectrolyte backbones we determine the axial profiles of the \perp - and \parallel -components of the corresponding radius of gyration and end-to-end distance.

1. Introduction

The adsorption of polyelectrolytes at solid–liquid interfaces plays a pivotal role in the formation of membranes and nanoscale layered films assembled by the layer-by-layer (LBL) technique.¹ Since the inception of this technique a variety of experimental studies have provided some insights into the mechanisms behind the membrane formation, including evidence that the backbone adsorption appears irreversible with no participation of counterions,² that the surface charge inversion proceeds via ion pairing between oppositely charged polyions,³ and that the membrane buildup might be tuned by adding salt of multivalent cations, by manipulation of polyion concentration,² and by the solvent quality.⁴

Although the body of experimental evidence is significant, the theoretical analysis of the deposition process and the success of the corresponding modeling effort are still limited.^{5–9} At least a couple of reasons lie behind this situation, namely, the intrinsic difficulties of interpreting and translating the experimental observations into working hypotheses and, then, the need for unambiguous connections between the microscopic details (embedded into the hypotheses) of the system and their macroscopic manifestation, that is, the formulation of the theory.

Molecular-based modeling of self-assembly of aqueous polyelectrolytes over solid substrates relies on the microscopic understanding of the relevant interactions among species in

solutions, as well as between those species and the substrates that translate into ion-pair formation and counterion condensation. This understanding becomes crucial in the design of novel systems with desired separation performance and is also a prerequisite to link this performance to the molecular architecture of the polyelectrolyte and the nature of the substrates, as well as the microstructure of the resulting interface. The behavior of the interface between a substrate and an aqueous polyelectrolyte solution results from a delicate balance between short-range (solvation) interactions characterizing the local environment around the species in solution and long-range (though partially screened by the presence of ions) electrostatic interactions leading to intrinsic as well as extrinsic charge compensation.^{3,10} In fact, this interfacial behavior is affected by a number of factors including the nature of the counterions and their electrostatic and short-range interactions with the polyelectrolyte binding sites, as well as their interactions with the solid substrate. Moreover, the local environment around the charged species depends strongly on the solvent's properties and the ionic strength, as well as the state conditions, and consequently, these domains are significantly different from those often characterized by a primitive (continuum dielectric) solvent.^{11,12}

All these features highlight the need for a more detailed understanding, beyond the traditional macroscopic treatments, of all relevant interactions with and within an explicit description of the solvent, the dissolved species, and the solid surface. In this context molecular-based simulation provides a direct route from the microscopic details of precisely defined interaction models to the macroscopic behavior of the systems and offers

* To whom correspondence should be addressed. E-mail: chialvoaa@ornl.gov. Fax: 865-574-4961.

[†] Aqueous Chemistry and Geochemistry Group.

[‡] Center for Nanophase Materials Sciences Division.

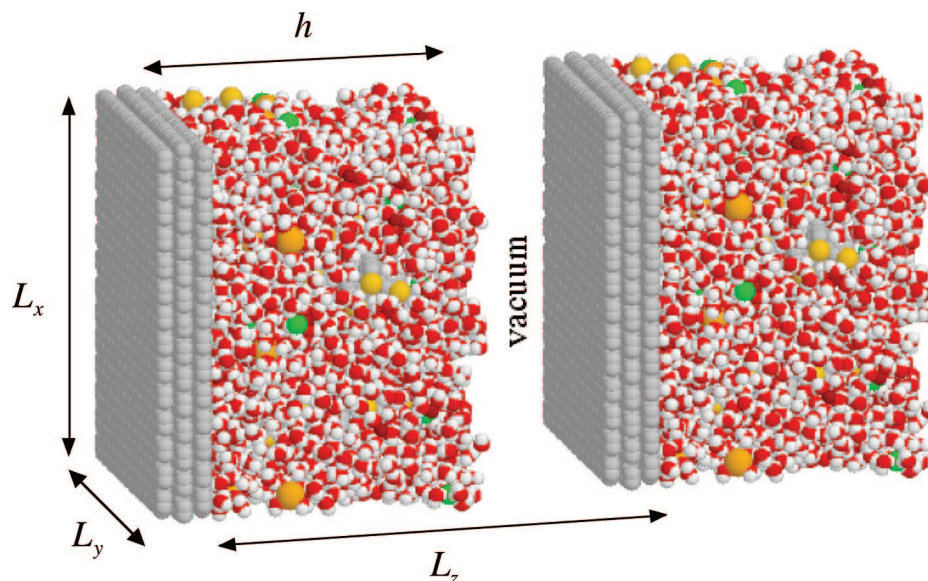


Figure 1. Geometry of the simulation cell under the EW3DLC periodic boundary conditions.

the unique opportunity for the testing of hypotheses embedded in the developments of theoretical formalisms and macroscopic modeling.

Obviously, the molecular simulation of these interfacial aqueous polyelectrolyte systems becomes a CPU-intensive task due to the coexistence of phenomena with rather different length¹³ and time scales.¹⁴ Yet, this approach has become a very powerful means to interpret the mechanisms of ion pair formation, counterion condensation, and their interplay underlying the behavior of polyelectrolyte solutions in the presence of salts. In fact, we were recently able to illustrate the connection between the ion pair formation and the counterion condensation in the appearance of like-charge interchain attractive interactions.¹²

What differentiates our study from other simulation efforts, including Messina's,^{15,16} Dobrynin et al.'s^{17–22} Terao's,^{23–25} and Yethiraj et al.'s^{26,27} is our explicit description of the polyelectrolyte chains, the ion-counterions, the solid surface, and more importantly, the atomistic account of the solvent water interactions with all species, that is, their concomitant solvation behavior. In fact, with the exception of the work of Reddy et al.'s, most simulation studies of polyelectrolyte adsorption on solid surfaces involved primitive models, where the counterions are either hard or soft sphere counterions interacting through dielectrically screened electrostatic interactions, that is, an implicit solvent represented as a continuum dielectric, and the polyelectrolyte backbones are bead-spring chains whose connectivity is maintained by a FENE potential.²⁸ The intrinsic inability of these models to describe the solvation behavior, that is, the distinct inhomogeneous local solvent environment around species, is probably one of the most significant defects of the primitive approaches and precludes the realistic representation of (hydrated) ion binding, pairing, and condensation.¹²

Therefore, the scope of our investigation comprises the following fundamental questions: (a) How strongly are the counterions adsorbed on the surface, and are they hydrated? (b) What role do the sulfonate groups play in the adsorption of counterions, and does this depend on the surface charge? (c) How effective is the screening of the surface charge by counterion adsorption? (d) What is the effect of the graphene surface on the ion-pair behavior of the added salt? (e) What is the conformational behavior of the polyelectrolyte backbones?

To address the proposed questions we perform extensive molecular dynamics simulations of precisely defined model systems, including the explicit and atomistic description of the solvent, according to the models and methodology presented in Section 2. In Section 3 we present and discuss the microstructural and conformational outcome of these molecular simulations in terms of the full characterization of the inhomogeneous environment at the solid–liquid interface, that is, the electric double layer (EDL) and the effect of the added salts (BaCl₂ and LaCl₃) on its structure. In addition, in the Supporting Information, we analyze the local environment around the ions to assess their solvation behavior, including their tendency to ion-pair formation, and estimate the strength of the adsorption of the polyelectrolyte, counterions, and other species in solution, to interpret the degree of surface-charge screening and the occurrence of surface-charge overcompensation and reversal. The microstructural description is supplemented by interpretation of the conformational behavior of the polyelectrolyte backbones based on the determination of the axial profiles for the \perp - and \parallel -components of the corresponding radius of gyration and end-to-end distance. Finally, in Section 4 we close the paper with some final remarks and outlook.

2. Potential Models and Simulation Methodology

The simulation cell was defined by a rectangular prism, with a rectangular base of dimensions $L_x = 58.22$ Å and $L_y = 54.10$ Å, comprising three graphene layers in the xy -plane at $z = 0$ and bounded by a containment wall represented by a WCA potential (whose parameters are similar to those for the Lennard-Jones representation of the carbon sites in the graphene wall)²⁹ at $z = h$, where h is chosen so that the nominal (geometrical) density of the system is approximately 1.0 g/cm³, that is, $48.12 \leq h$ (Å) ≤ 49.54 (see Figure 1). The first layer of the graphene wall at $z = 0$, that is, in contact with the aqueous solution, might bear some small partial charge, either uniformly or randomly distributed on each carbon site, compensated by ions from the added salts in the solution. This simulation configuration not only depicts the actual experimental setup but also, as opposed to a slit geometry where two walls are needed, allows us to study the adsorption phenomenon avoiding the potential effect of confinement without resorting to larger h and, consequently, larger CPU requirements.

TABLE 1: Surface Charge and Composition of Aqueous Li⁺PSS[−]–Electrolyte Solutions

σ_s , C m ^{−2}	q_s^a	N_{Li^+}	$N_{\text{Ba}^{2+}}$	$N_{\text{La}^{3+}}$	N_{Cl^-}	$N_{\text{H}_2\text{O}}$	$N_{\text{SO}_3^-}$
−0.101	−20	100		20	60	4000	80
−0.101	−20	100	20		40	4000	80
0	0	100		20	80	4000	80
0	0	100	20		60	4000	80
0	0					4000 ^b	
+0.101	20	100		20	100	4000	80
+0.101	20	100	20		80	4000	80

^a Total electrostatic charge at carbon sites exposed to the fluid phase. ^b Pure water in contact with the graphene wall.

To account properly for the electrostatic interactions under this 2D periodic geometry, we implemented a very efficient 3D Ewald summation with an electric layer correction, EW3DLC,^{30–32} involving a real-space cutoff radius $r_c = 0.35(h + h_w)$ (where h_w denotes the thickness of the wall) with the corresponding optimal values for the reciprocal-space cutoff of $k_c = 8$, the Ewald third dimension $L_z = 1.2(h + h_w)$, and convergence parameter $\alpha(h + h_w) \cong 7.8$, respectively, to achieve an error of the order of 10^{-5} for the Coulombic energy and forces according to the analysis of Brodka.^{33,34} Note that a change in L_z , from $L_z = 1.2(h + h_w)$ to $L_z = 2.0(h + h_w)$, has a negligible effect on the optimal value of α . We should note that, because of the more accurate expressions for the estimation of the errors in the forces and energy, as well as its underlying slab-wise summation, the EW3DLC requires much smaller L_z and correspondingly k_c values than those for the alternative 3D Ewald summation, EW3DC.³⁵

We have performed isothermal–isochoric molecular dynamics (NVT-MD) simulations of aqueous polyelectrolyte solutions comprising 4000 water molecules, 10 polystyrene sulfonate (PSS) octamers, the corresponding Li⁺ counterions, and added salts (such as Cl₂Ba or Cl₃La) in contact with a graphene wall. When salt was added to the system in order to study the effect of polyvalent cations on solvation behavior, chloride ions were used to maintain the systems' electroneutrality (see Table 1). As for our previous study,¹² the PSS octamers were 100% sulfonated chains, water was described by the SPC/E model,³⁶ Li⁺ and Ba²⁺ according to Åqvist,³⁷ Cl[−] according to Smith and Dang,³⁸ and La³⁺ by van Veggel's parametrization,³⁹ respectively.

The graphene wall was composed of three graphitic layers stacked on top of each other and perpendicular to the z -direction with an interlayer separation of 3.35 Å, with an adjacent carbon–carbon distance of 1.42 Å, with the carbon sites explicitly described as Lennard-Jones spheres characterized by $\epsilon_{\text{CC}}/k = 28$ K and $\sigma_{\text{CC}} = 3.40$ Å.⁴⁰ All unlike interaction parameters for the Lennard-Jones potentials between species in solution and the graphene are determined by the corresponding Lorentz–Berthelot combining rules.

While graphene sheets are normally electroneutral, it is possible to induce surface charges by chemical doping with nitrogen (positive charges) and boron (negative charges),⁴¹ as well as by covalent attachment of ligands such as $-\text{CO}_2^-$ and $-\text{NH}_4^+$.⁴² For that purpose, in our study the charged surfaces are modeled by distributing the total charge equally over each carbon site on the innermost graphitic layer and their interactions with other charged species accounted for by the EW3DLC method.

The NVT-MD simulations were performed by implementing the Martyna-Tuckermann-Klein (MTK) explicit reversible integrator,⁴³ following Cheng and Merz's scheme⁴⁴ except for the

use of a single SHAKE-routine call scheme suggested by Palmer⁴⁵ as opposed to the original dual SHAKE⁴⁶-RATTLE⁴⁷ routine calls. This substitution becomes an efficient scheme to fulfill all constraints and their time-derivatives, simultaneously, and successfully applied in our earlier simulation studies of ion-pair formation and counterion condensation.^{12,48,49}

In all cases the initial configurations (random distribution of species) were generated by the *Packmol* routine⁵⁰ and then equilibrated for at least 0.5 ns prior to the accumulation of the corresponding quantities for the calculation of their averages, over 4.5 ns of phase-space trajectory, using a time-step size of 2.0 fs. Because these are very CPU-demanding simulations, we have doubled the simulation time on a few runs to check the equilibration of the resulting profiles and concluded that the interfacial structures were completely developed at 4.5 ns. These quantities comprised the conformational properties of the octamers, such as the axial profiles of the parallel and perpendicular components of the radius of gyration (see eq 4 below) and the corresponding to the end-to-end distance (see eq 5 below), as well as the configurational properties of the solutions, including the site–site radial distribution functions for water–water, ion–water, ion–chain, chain–water, and chain–chain interactions. In addition to the usual kinetic temperature and to verify the proper conformational and configurational equilibration, we have monitored the configurational temperatures⁵¹ (see appendix A of Chialvo and Simonsen¹² for details). All simulations were run on a parallel architecture using our parallel (MPI) algorithm based on a replicated data approach.^{52,53}

To characterize the structure of the graphene–aqueous interface and to interpret the behavior of the EDL, we determine the axial profiles of all species concentrations $\rho_i(z)$, the corresponding Coulombic charge density $\rho_Q(z)$ and relative orientation of the water molecules $\rho_\theta(z)$ as follows:

$$P(z) \equiv \left\langle (L_x L_y \Delta)^{-1} \sum_i P_i B_c(z_i, -0.5\Delta, +0.5\Delta) \right\rangle \quad (1)$$

where $B_c(x, a, b) \equiv [\Theta(x - a) - \Theta(x - b)]$ is the “boxcar” function,⁵⁴ P_i denotes $\delta(z - z_i)$, the Coulombic charge q_i , and the angle $\theta = \cos^{-1}(\mu_i \cdot \hat{z}/|\mu_i|)$, respectively, where μ_i is the dipole moment of the water molecule i , L_α represents the size of the simulation box along the α -axis, $\Delta \sim 0.3$ Å, and the $\langle \dots \rangle$ indicates a time average over the simulation trajectory.

In particular, the axial profile of the charge density $\rho_Q(z)$ plays a central role in this analysis, since the integration of the associated one-dimensional Poisson equation provides the corresponding profiles for the local electric field and potential. These profiles afford the opportunity to assess how effective the solution screens the surface charge, especially at the EDL domain, where the possibility of either overcharging or surface charge reversal might occur. To analyze this scenario we define the strength of the surface charge (σ_s) screening, $\mathcal{S}(z) \equiv -\sigma(z)/\sigma_s$, where

$$\sigma(z) = \int_0^z \rho_Q(z) dz \rightarrow \sigma(h) = \int_0^h \rho_Q(z) dz \quad (2)$$

Moreover, by invoking the condition of electroneutrality, $\sigma(h) = -\sigma_s$, and from Gauss' law,⁵⁵ this surface charge is proportional to the electric field $E(z)$ strength at the interface, that is,

$$E(z) = -4\pi \int_z^h \rho_Q(z) dz = 4\pi[\sigma(z) - \sigma(h)] \quad (3)$$

so that $\sigma_s = E(0)/4\pi$. Consequently, we can also write $\mathcal{S}(z) = [E(0) - E(z)]/E(0)$. The main feature of this axial function is its ability to portray how effectively the aqueous electrolyte

screens the surface charge, bounded by the two obvious conditions, that is, null-screening, $\mathcal{A}(0) = 0$, and full-screening, $\mathcal{A}(h) = 1$. However, we are most interested in the screening behavior between these two limiting cases, especially in the neighborhood of the solid–liquid interface, where the EDL’s geometry arises from a delicate balance of species’ solvation and binding interactions (adsorption) with the surface (see discussion below).

To interpret the effect of the graphene surface on the conformation of the oligomer chains we determine the average profiles of the parallel ($R_G^{\parallel}(z)$) and perpendicular ($R_G^{\perp}(z)$) components of the radius of gyration as well as the corresponding for the end-to-end distance, *i.e.*, $R_{ee}^{\parallel}(z)$ and $R_{ee}^{\perp}(z)$, respectively, where z is the axial distance from the graphene wall to the center of mass of the chain, that is,

$$R_G^{\parallel}(z) = \langle B_c(z_{com}, -0.5\Delta, +0.5\Delta) \sum_i m_i [(x_i - x_{com})^2 + (y_i - y_{com})^2] \Big/ \sum_i m_i \rangle^{0.5}$$

$$R_G^{\perp}(z) = \langle B_c(z_{com}, -0.5\Delta, +0.5\Delta) \sum_i m_i (z_i - z_{com})^2 \Big/ \sum_i m_i \rangle^{0.5} \quad (4)$$

where $(r_i - r_{com})$ is the position of site i relative to the oligomer’s center of mass r_{com} , m_i is the corresponding site mass, $B_c(\dots)$ is the “boxcar” function defined earlier, and $\langle \dots \rangle$ denotes a simulation average. Likewise,

$$R_{ee}^{\parallel}(z) = \langle [(x_1 - x_N)^2 + (y_1 - y_N)^2] B_c(z_{com}, -0.5\Delta, +0.5\Delta) \rangle^{0.5}$$

$$R_{ee}^{\perp}(z) = \langle (z_1 - z_N)^2 B_c(z_{com}, -0.5\Delta, +0.5\Delta) \rangle^{0.5} \quad (5)$$

where $(r_1 - r_N)$ is the relative position of one end of the chain with respect to the other end.

3. Microstructural and Conformational Results

In this section we present the structural and conformational behavior of the system, with particular emphasis on that at the interfacial region, discuss the resulting solid–liquid interface structure, and interpret the resulting surface–charge screening and reversal in terms of the strength of ion adsorption. All these profiles were determined after the systems were properly equilibrated, kinetically and configurationally, as illustrated in Figure 2.

3.1. Interfacial Structure. In order to interpret the effect of the graphene wall on the interface structure, we first analyze the system comprising only water as opposed to the aqueous polyelectrolyte solution. In Figure 3 we display the axial profiles

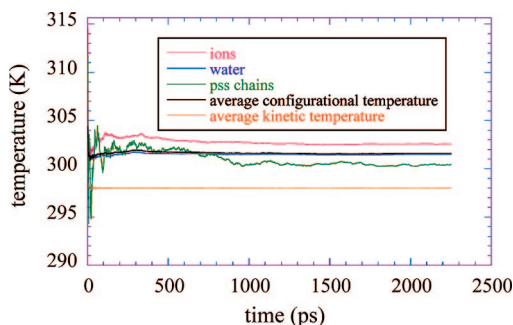


Figure 2. Time evolution of the average configurational temperature, its individual contributions, and the corresponding kinetic temperature of the thermostatted system.

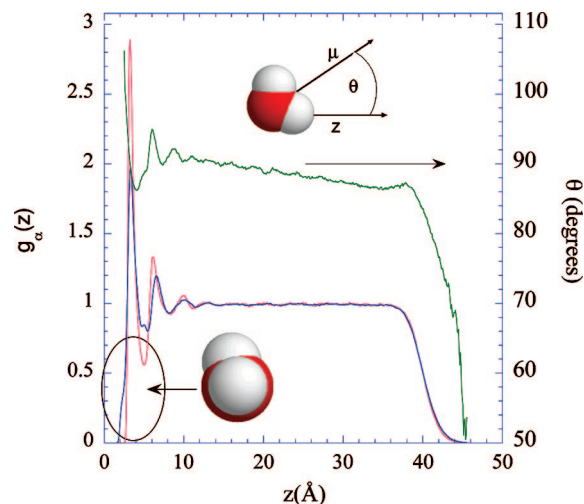


Figure 3. Comparison of the axial profiles of the water sites and relative dipole orientation for pure water in contact with a neutral and uncharged graphene surface.

of the water structure (*i.e.*, oxygen and hydrogen sites) and corresponding relative orientation of the water’s dipole moment, $\theta = \cos^{-1}(\mu_i \cdot \hat{z} / |\mu_i|)$, where we can clearly observe the formation of three water layers within 12 Å from the graphene surface, beyond which water exhibits no axial structure. Moreover, according to this orientational profile, the water molecules lie in planes, defined by their three sites, quasi-parallel to the wall; that is, the axial locations of the oxygen and hydrogen peaks roughly coincide. Note however that there is a small tilt of one of the water hydrogens toward the graphene wall (see inset of Figure 3).

As soon as we introduce the polyelectrolyte into the solution and eventually a neutralizing salt for the case of charged graphene walls, we observe significant changes in the axial structure (*e.g.*, Figure 4a–c for added BaCl_2 and Figure 5a–c for added LaCl_3). The first and most obvious, though weak, is the disruption of the axial uniform distribution of water for $z > 12$ Å. This effect is caused by the backbone connectivity of the polyelectrolyte chains and the differential solvation behavior between the hydrophilic sulfonate groups and the hydrophobic backbones. Moreover, as we will discuss below, the differential interaction between ions and the graphene wall, that is, ion adsorption, contributes to the distortion of the original water layering, whose effect is magnified by the presence of the charged surface. The second evident structural change is the pronounced reorientation of the innermost layer of interfacial water as the surface charge goes from positive to negative, whose manifestation is the splitting of a original hydrogen site peak (located either at ~ 3.2 Å for BaCl_2 added or ~ 3.3 Å for LaCl_3 added) into two peaks roughly located at ~ 2.1 Å and ~ 3.37 Å from the graphene layer (see Figures 4c and 5c).

To find the mechanism underlying this behavior, we now analyze the axial profiles of ion concentrations in comparison with the corresponding water sites (Figure 6a–c and Figure 7a–c) for solutions with BaCl_2 and LaCl_3 added, respectively). Starting with the neutral graphene surface, we note that because of its small size and water coordination, $n_{\text{O}}^{\text{Li}^+} \approx 4$ (see Supporting Information), Li^+ is able to adsorb significantly through a water-mediated mechanism at about 4 Å from the wall. Yet, despite having a larger charge, Ba^{2+} cannot get closer (than Li^+) to the graphene due to its larger water coordination, that is, $n_{\text{O}}^{\text{Ba}^{2+}} \approx 8$ (see Supporting Information), but more importantly, because it is hindered by the strong counterion condensation on the $-\text{SO}_3^-$

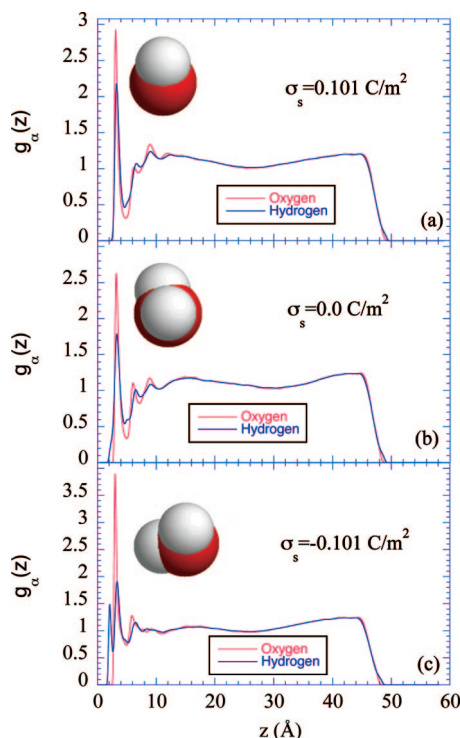


Figure 4. Comparison of the axial profiles of the water sites for aqueous Li^+PSS^- solutions with added BaCl_2 in contact with a charged graphene surface: (a) $\sigma_s = 0.101 \text{ C/m}^2$, (b) $\sigma_s = 0.0 \text{ C/m}^2$, and (c) $\sigma_s = -0.101 \text{ C/m}^2$.

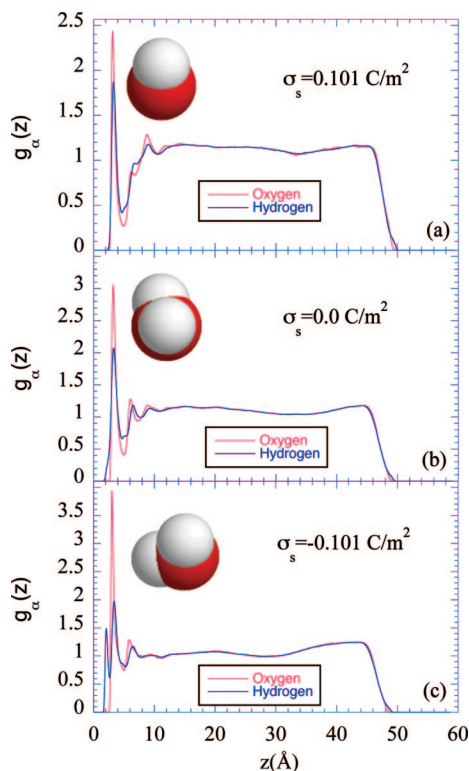


Figure 5. Comparison of the axial profiles of the water sites for aqueous Li^+PSS^- solutions with added LaCl_3 in contact with a charged graphene surface: (a) $\sigma_s = 0.101 \text{ C/m}^2$, (b) $\sigma_s = 0.0 \text{ C/m}^2$, and (c) $\sigma_s = -0.101 \text{ C/m}^2$.

groups which become sandwiched between the Li^+ and the Ba^{2+} at about 4.7 Å from the graphene surface (Figure 6b). In fact, the Ba^{2+} adsorption exhibits a rather weak peak at 5.3 Å and a stronger second peak at about 8 Å from the neutral surface.

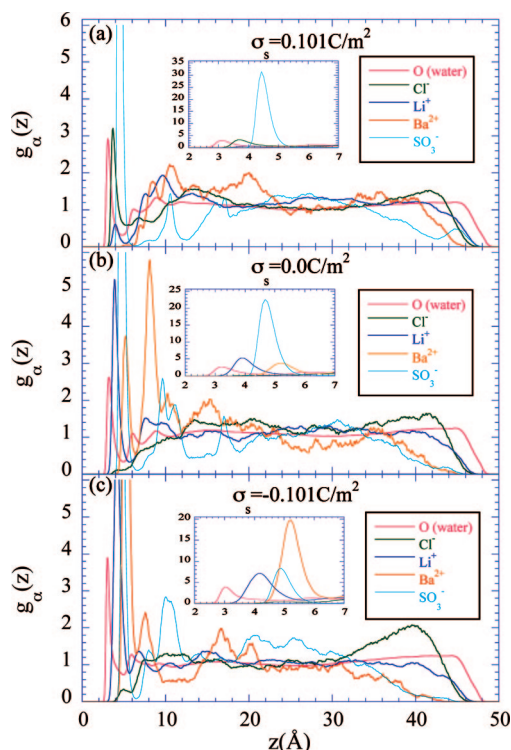


Figure 6. Comparison of the axial profiles of species distribution functions in aqueous Li^+PSS^- solutions with added BaCl_2 in contact with a charged graphene surface: (a) $\sigma_s = 0.101 \text{ C/m}^2$, (b) $\sigma_s = 0.0 \text{ C/m}^2$, and (c) $\sigma_s = -0.101 \text{ C/m}^2$.

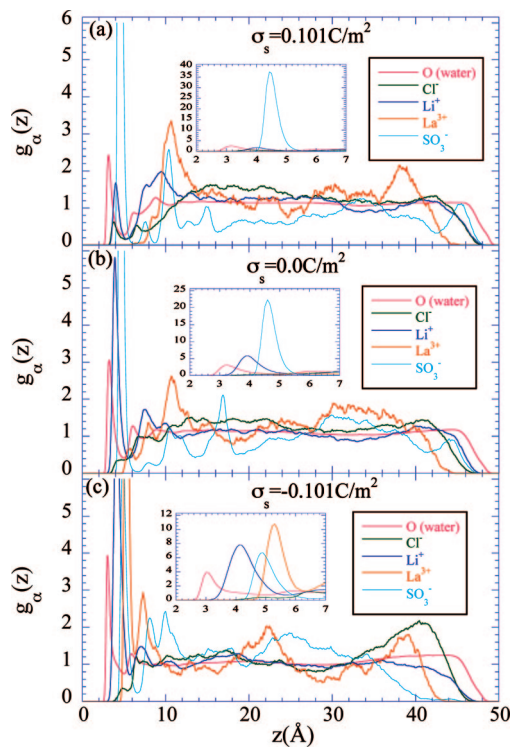


Figure 7. Comparison of the axial profiles of species distribution functions in aqueous Li^+PSS^- solutions with added LaCl_3 in contact with a charged graphene surface: (a) $\sigma_s = 0.101 \text{ C/m}^2$, (b) $\sigma_s = 0.0 \text{ C/m}^2$, and (c) $\sigma_s = -0.101 \text{ C/m}^2$.

Note also that, because the adsorption of Cl^- ($n_{\text{Cl}^-}^0 \approx 7.5$) occurs at about the same distance as the $-\text{SO}_3^-$ groups ($n_{\text{SO}_3^-}^0 \approx 8.2$), Cl^- is barely adsorbed on the neutral graphene, under the competition from the $-\text{SO}_3^-$ groups aided by the condensation of cations.

As expected, the charging of the graphene surface modifies the interfacial structure, by adjusting the strength of the species adsorptions, balanced by the strength of the ion-pairing and counterion condensation. In the case of added LaCl_3 we observe significant differences in the adsorption of the polyvalent counterion, that is, La^{3+} versus Ba^{2+} as depicted in Figure 7a–c. In fact, considering that both cations involve very similar non-Coulombic forcefields (see Table B1 of ref 12), the negligible adsorption of La^{3+} compared to Ba^{2+} on the neutral surface at $z \sim 6 \text{ \AA}$ may be ascribed to its larger water coordination, that is, $n_{\text{O}}^{\text{La}^{3+}} \approx 9$ versus $n_{\text{O}}^{\text{Ba}^{2+}} \approx 8$.

3.2. Screening of Surface-Charge by the Electrolyte.

Obviously, the axial profiles of species concentrations depicted in Figures 4–7 are more detailed representations of the inhomogeneous environment than those from the axial profiles of the charge density, that is, the latter result from the summation of the individual contribution of the former weighted by the corresponding species charges, $\rho_Q(z) = \sum_i x_i q_i \rho_i(z)$ (see also eq 1). Yet, the charge density profiles provide a more revealing picture of the local charge cancellation, the global electroneutrality of the system, and ultimately, of the degree of surface-charge screening by the aqueous electrolyte solution. Moreover, by integration of the one-dimensional Poisson equation for the simulated charge density profile we extract the corresponding electric field profile, and consequently, we can link the adsorption strength of the individual ions with the distortion of the electric field of water at the graphene/water interface, and the concomitant degree of local charge screening.

In Figures 8a,b and 9a,b we display the axial profiles for the charge densities and the corresponding electric fields for the two sets of systems (i.e., with added BaCl_2 and LaCl_3 , respectively) in comparison to that for the reference pure water system in contact with the uncharged graphene wall. Figures

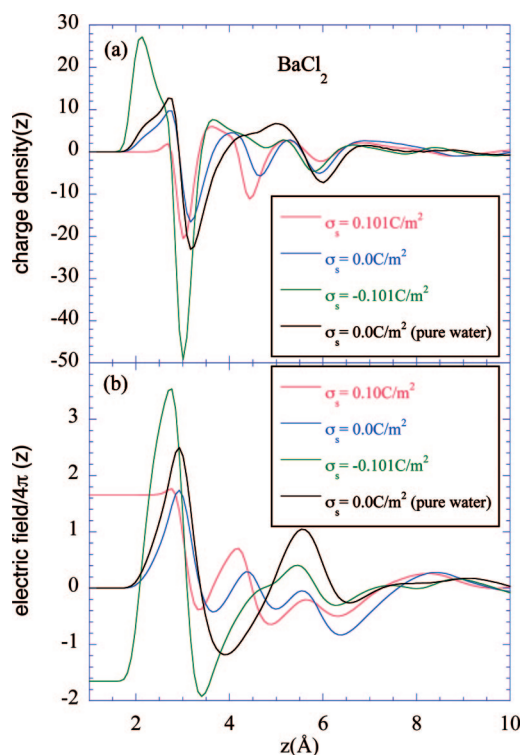


Figure 8. Comparison of axial profiles for (a) the charge density and (b) electric field in aqueous Li^+PSS^- solutions with added BaCl_2 in contact with a graphene wall bearing a surface charge σ_s . Charge density and electric field in $(\sigma_{\text{SPCE}}^3/\epsilon_{\text{SPCE}})^{0.5}$ and $(\sigma_{\text{SPCE}}/\epsilon_{\text{SPCE}})^{0.5}$ units, respectively.

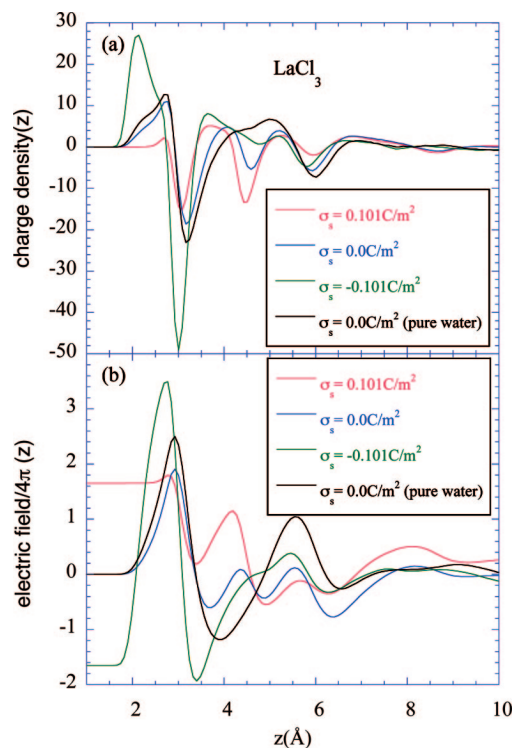


Figure 9. Comparison of axial profiles for (a) the charge density and (b) electric field in aqueous Li^+PSS^- solutions with added LaCl_3 in contact with a graphene wall bearing a surface charge σ_s . Charge density and electric field in $(\sigma_{\text{SPCE}}^3/\epsilon_{\text{SPCE}})^{0.5}$ and $(\sigma_{\text{SPCE}}/\epsilon_{\text{SPCE}})^{0.5}$ units, respectively.

8a and 9a provide a clear picture of the distortion of the charge distribution due to the adsorption of Li^+ , Ba^{2+} , La^{3+} , and $-\text{SO}_3^-$ within $2 \text{ \AA} < z < 6 \text{ \AA}$ from the graphene surface. In particular, note the appearance of an additional peak (and valley) in the distribution $\rho_Q(z)$ with respect to that for electrolyte-free system (i.e., pure water and $\sigma_s = 0.0 \text{ C/m}^2$) and the remarkable similarity between the profiles for the systems containing BaCl_2 and LaCl_3 . This similarity is also evident in the corresponding electric field axial profiles, Figures 8b and 9b, where the ion adsorption is clearly manifested by the presence of an additional peak around $z \approx 4 \text{ \AA}$, sandwiched between the two original peaks located at $z \approx 3 \text{ \AA}$ and $z \approx 5.5 \text{ \AA}$. Note also that the strength of this third peak depends on the sign of the graphene surface charge σ_s ; that is, it becomes stronger as the surface charge goes from $\sigma_s < 0$ to $\sigma_s > 0$.

Here we should highlight the occurrence of a new phenomenon, referred to as overcharging (OC) by Lozada-Cassou and Jimenez-Angeles,⁵⁶ who first reported it for the adsorption of primitive model macroions onto planar charged-surfaces, that is, when the first layer of adsorbed species increases the surface charge as oppose to screens it. In particular, note the small but clear peak at $z \sim 2.8 \text{ \AA}$ in the profiles of the charge density and corresponding electric field strength (\sim net charge per unit of lateral surface) in Figures 9a,b–11a,b for $\sigma_s > 0$ (red curve), that bear a clear resemblance to that in the inset of Figure 2 in ref 56, despite the obvious significant differences between the two types of systems. In fact, the contrasting differences between our system, where all species are atomistically described including the explicit inclusion of the solvent water, and that of Jimenez-Angeles and Lozada-Cassou,⁵⁶ where the ions are charged hard-spheres immersed in a dielectric continuum representing implicitly the solvent water, pushes for an understanding of the underlying mechanism for the overcharging and

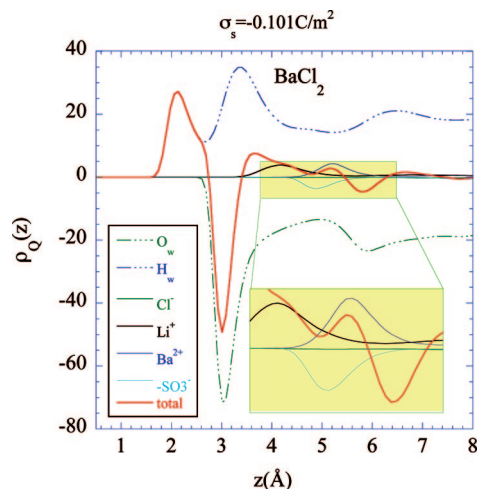


Figure 10. Individual species contributions to the total charge density axial profile for the aqueous Li^+PSS^- solution with added BaCl_2 in contact with a graphene wall bearing a surface charge $\sigma_s = -0.101 \text{ C/m}^2$. Charge density in $(\sigma_{\text{SPCE}}^3/\epsilon_{\text{SPCE}})^{0.5}$ units.

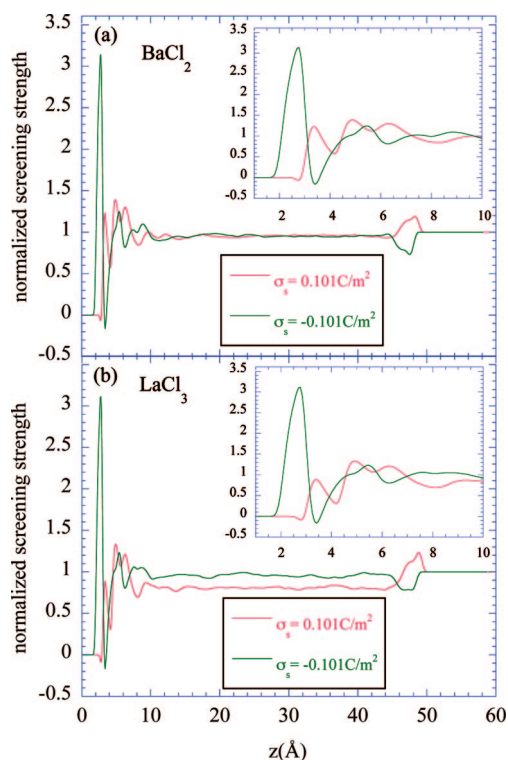


Figure 11. Comparison of axial profiles for normalized screening strength $\mathcal{A}(z)$ in aqueous Li^+PSS^- solutions in contact with a graphene wall bearing a surface charge σ_s : (a) added BaCl_2 and (b) added LaCl_3 .

concomitant charge reversal. For that purpose we plot in Figure 10 the individual components $\rho_Q(z) = x_i q_i \rho_i(z)$ involved in $\rho_Q(z) = \sum_i x_i q_i \rho_i(z)$, for the representative case of $\sigma_s = -0.101 \text{ C/m}^2$ with BaCl_2 added, to identify their contributions to each relevant peaks in the axial profiles of the charge density and electric field. This picture indicates that the two main sources of charge screening in the innermost region of the solid/aqueous interface are the water–oxygen and water–hydrogen sites, whose effective interactions with the surface would determine the relative orientation of water with respect to the graphene layer, and ultimately, the relative axial location of these charged sites (see insets in Figures 3–5). In fact, the first peak of $\rho_Q(z)$ (positive) is associated with the water–hydrogen site closer to the graphene

surface and is followed by a deep valley (negative) corresponding to the water–oxygen site as well as the second (partially screened) water–hydrogen site (positive), whose tail is modified by the contribution from the adsorbed Li^+ . Note that for this case, $\sigma_s < 0$, the negative contribution from the adsorbed $-\text{SO}_3^-$ is rather weak and sandwiched (screened) by the positive contributions of Li^+ and Ba^{2+} (inset of Figure 10). As we change the surface charge from $\sigma_s < 0$ to $\sigma_s > 0$, we observe that the strong first peak and valley of $\rho_Q(z)$ are significantly reduced, as the orientation of the adsorbed water molecules changes (insets of Figures 4 and 5), while the second valley becomes deeper.

These electric field profiles translate into remarkable screening counterparts as illustrated in Figure 11a,b, where we compare the charge-screening behavior, $\mathcal{A}(z)$, of the aqueous electrolyte–polyelectrolyte systems for the same magnitude of surface charge, but opposite signs. By recalling that $\mathcal{A}(z) = 0$ and $\mathcal{A}(z) = 1$ denote null and full screening, respectively, the outstanding feature of these profiles is the obvious overcompensation of the surface charge within $z < 4 \text{ Å}$, that is, a reversal of the local surface charge followed by an oscillatory screening behavior within the region of the three water layers.

Figure 11a,b also reveals that, while the cations are able to screen effectively the negative surface charge within 10 Å from the surface, the anions are not. This behavior must be traced back to the different solvation behavior of these species and the connectivity of the charged sites in the chain backbones, as well as the interplay between counterion condensation and ion pair formation, that ultimately prevents the charged species from approaching closer to the charged graphene surface.

3.3. Chain Conformation. The profiles of conformational properties suggest the formation of water- and counterion-mediated chain layers, resembling those in the extrinsic charge compensation scheme³ but involving similar chain backbones. The behavior of the axial profiles of the \parallel - and \perp -components of the squared radius of gyration and end-to-end distance, Figure 12, indicates layering of chain's backbones parallel to the graphene surface. Because of the intrinsic negative charge of these chains, though partially screened by the condensed cations,¹² the chain–graphene interactions are strongest for $\sigma_s > 0$ (e.g., Figure SI-5(b) of Supporting Information), whose conformational manifestation is an increase of the asymmetry of the \parallel - and \perp -components of $R_G(z < 10 \text{ Å})$ and $R_{ee}(z < 10 \text{ Å})$. This effect, accentuated by the charging of the graphene surface, can be clearly visualized in terms of a loosely defined form-factor $\mathcal{R}(z) \equiv 0.5R_G^{\parallel 2}(z)/R_G^{\perp 2}(z)$ so that $\mathcal{R}(z) \approx 1$, that is, $R_G^{\perp 2}(z) = R_G^{\parallel 2}(z)/2 \approx R_G^2(z)/3$ represents a bulk-like behavior, while $\mathcal{R}(z) > 1$ would indicate a flattening of the chains as they are compressed against the graphene wall. Figure 13 illustrates this behavior and suggests that the interaction of these short chains with the graphene wall induces some significant flattening within 10 Å from the surface, even when the graphene surface is uncharged, and then the chains behave approximately as in a bulk solution.¹² Note that for $\sigma_s < 0$ the chain flattening is dramatically reduced as we might have expected considering the less favorable net chain–wall interactions.

4. Discussion and Final Remarks

The target of this investigation has been the interfacial behavior of short-chain lithium polystyrene-sulfonate aqueous solutions in contact with graphene surfaces, in the presence of multivalent cations and discrete surface charges. For that purpose, we have placed emphasis on the explicit and realistic description of the water, the chain backbones, and species in

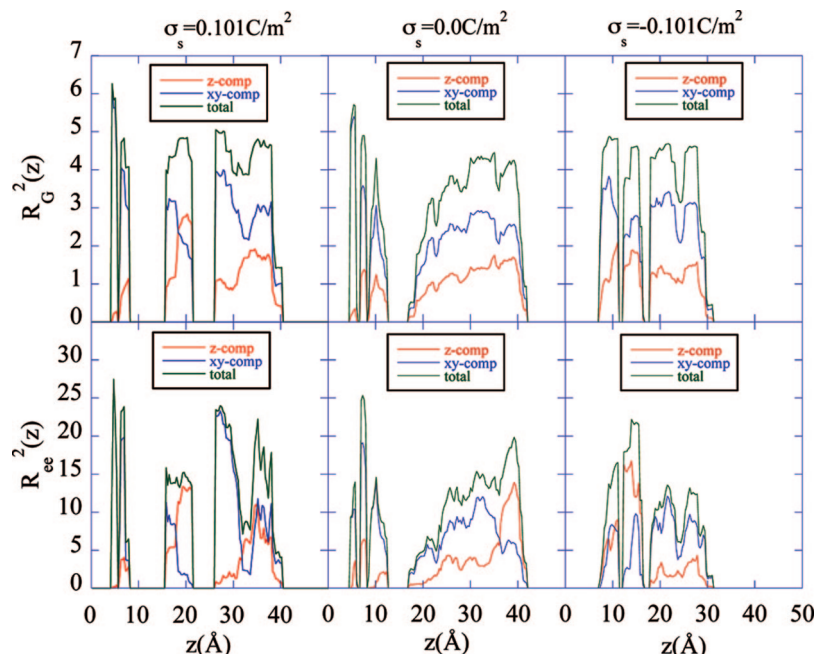


Figure 12. Effect of the surface charge (with addition of LaCl_3) on the axial profiles of the \perp - and \parallel -components of (a) the squared radius of gyration and (b) the squared end-to-end distance of the aqueous PSS[−] chains in contact with the graphene surface. $R_G^2(z)$ and $R_{ee}^2(z)$ in units of $\sigma_{\text{SPCE}}^{-2}$.

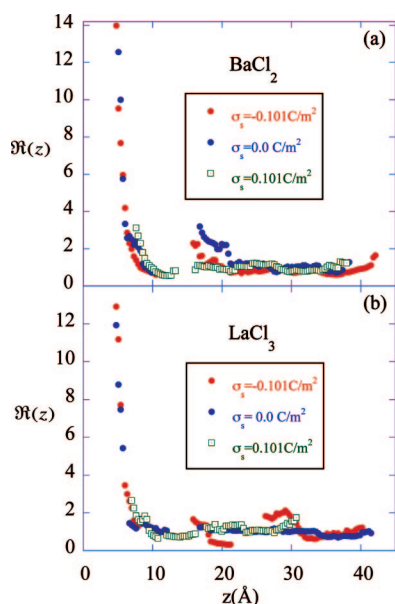


Figure 13. Axial profile of the ratio $\mathcal{R}(z)$ between the \perp - and \parallel -components of the squared radius of gyration of the aqueous PSS[−] chains in contact with the graphene surface.

solution to analyze the formation of the EDL, the concomitant screening of the surface charge by the surrounding aqueous environment, and the possible mechanism underlying overcharging and surface charge reversal. Moreover, to aid the interpretation of the surface-charge screening mechanism, we have analyzed the corresponding solvation behavior of the relevant species within slabs parallel to the graphene surface.

According to the analysis and discussion of the previous sections we now can address the questions proposed in the introduction by summarizing the relevant results:

(a) All ions are adsorbed as hydrated species following the order of adsorption strength from $\text{Ba}^{2+} > \text{La}^{3+} > \text{Li}^+ > -\text{SO}_3^- \gg \text{Cl}^-$ for the negative-charged graphene surface, to $-\text{SO}_3^- > \text{Li}^+ > \text{Ba}^{2+} \approx \text{La}^{3+} \gg \text{Cl}^-$ for the neutral graphene surface,

and ending as $-\text{SO}_3^- > \text{Cl}^- (\text{Ba}^{2+}) > \text{Li}^+ > \text{Cl}^- (\text{La}^{3+}) \gg \text{Ba}^{2+} \approx \text{La}^{3+}$ for the positive-charged graphene surface, where $\text{Cl}^- (\text{M}^{z+})$ denotes the source (added salt) of the Cl^- (note that Figure SI-5 (Supporting Information) provides a more detailed account of these trends).

(b) The sulfonate groups play a crucial role in the adsorption of cations, in addition to their own interaction with the graphene surface, by the concurrent condensation of Li^+ and either Ba^{2+} or La^{3+} , a process that partially screens the intrinsic negative charge of the chains. This mechanism results in a net quasi-linear dependence of the adsorption strength with the surface charge of the graphene wall, whose slope depends on the charge of the multivalent cation.

(c) The graphene surface charge is indirectly screened by the adsorption of hydrated cations, that is, water mediated, by distorting the microstructure of the adsorbed water and aided by their condensation onto the adsorbed sulfonated chains. This mechanism contrasts with that involving the primitive model counterpart, where the surface charge is screened by ions in direct contact with the surface.

(d) The comparison between the behaviors depicted in Figures SI-3 and SI-4 (Supporting Information) indicate that the graphene surface-charge has opposite effects on the ion pairing compared to that on the counterion condensation, that is, an apparent odd behavior if we consider that both phenomena are pairing processes. However, this result is consistent with the conformational behavior of the chain's backbones (Figure 13) in that, as the surface-charge becomes negative, the backbones are axially compressed as they are pulled by the adsorption of the cations either surrounding or already condensed onto the sulfonate groups. The combination of this axial compression that makes possible a tighter cation–sulfonate condensation, with the unfavorable graphene– Cl^- interactions (Figures 6 and 7) that hinders closer cation– Cl^- encounters, is a plausible mechanism behind the observed contrasting behavior.

(e) The presence of the graphene wall, even if uncharged, has a profound impact on the conformation of the chain backbones with a clear tendency toward layering, resulting from

the concurrence of solvent-mediated chain adsorption onto the wall and (hydrated) counterion-mediated chain–chain interactions.

In addition, we have illustrated that the charge inversion in the adsorption of short-chain polystyrene–sulfonate onto charged surfaces originates on the induced orientational structure of the interfacial water, where the water's hydrogens and oxygens form two parallel planes with opposite density charges, while the adsorbed polyelectrolyte and counterions only contributes marginally, beyond the enforcement of electroneutrality. This picture should not be a surprise if we consider that (i) water is mediating all species interactions with the graphene surface, (ii) it is the most numerous species in the system, and (iii) as a strong dipolar species, water is described in terms of interconnected partial charges. However, this picture contrasts to that drawn by the theory and simulation of primitive models, where the solvent has the more passive role of screening the Coulombic interactions by a factor given by the chosen dielectric permittivity, and consequently, the charge inversion results from the balance of charge density asymmetries between anion and cations.^{57,58}

Obviously we could argue that water is an electroneutral polar species whose charged sites play the same role as those of other charged species such as either the counterions or the polyelectrolyte's charged sites, but its solvation power hinders other species from approaching the surface. In other words, while the mechanism of overcharging in our system appears analogous to that proposed by Jimenez-Angeles and Lozada-Cassou⁵⁶ (see insets of their Figure 2), we must point out significant conceptual differences with the latter, namely: the magnitude of the charges involved in our system are much smaller, that is, $q_{H_w} = 0.4238e = -0.5q_{O_w}$ as opposed to $q_M = -40e = -20q_+ = 40q_-$ in ref 56 resulting in a charge asymmetry of 2 compared to 20 in ref 56), and more importantly, in our case the charges are linked by the intramolecular O–H bond interactions in addition to the intermolecular O···H (hydrogen) bond interactions. A more detailed analysis on this phenomenon is underway and will be reported elsewhere.⁵⁹

Acknowledgment. This research was sponsored by the Division of Chemical Sciences, Geosciences, and Biosciences, Office of Basic Energy Sciences under Contract Number DE-AC05-00OR22725 with Oak Ridge National Laboratory, managed and operated by UT-Battelle, LLC. A.A.C. expresses his gratitude to Prof. Aleksander Brodka (Silesian University, Katowice, Poland), as well as Dr. Axel Arnold (Max Planck Inst., Mainz, Germany) and Dr. Jason De Joannis (Emory University, Atlanta) for private communications regarding the implementation of their methods.

Note Added after ASAP Publication. There was an error in eq 4 and in the equation in the first paragraph of section 3.1. The original version was published November 17, 2008, and the corrected version was posted December 4, 2008.

Supporting Information Available: Behavior of the water–water, ion–water, and ion–counterion in-plane distribution functions, as well as the strength of the species adsorption onto the graphene wall, including their analysis and five figures. This information is available free of charge via the Internet at <http://pubs.acs.org>.

References and Notes

- Decher, G.; Hong, J. D. *Makromol. Chem., Macromol. Symp.* **1991**, 46, 321.
- Lowack, K.; Helm, C. A. *Macromolecules* **1998**, 31, 823.
- Schlenoff, J. B.; Ly, H.; Li, M. *J. Am. Chem. Soc.* **1998**, 120, 7626.
- Dubas, S. T.; Schlenoff, J. B. *Macromolecules* **1999**, 32, 8153.
- Shafir, A.; Andelman, D. *Eur. Phys. J. E* **2006**, 19, 155.
- Lefauve, C. J.; Zimmerlin, J. A.; Dobrynin, A. V.; Mather, P. T. *J. Polym. Sci., Part B: Polym. Phys.* **2004**, 42, 3654.
- Netz, R. R.; Joanny, J. F. *Macromolecules* **1999**, 32, 9013.
- Castelnovo, M.; Joanny, J. F. *Langmuir* **2000**, 16, 7524.
- Park, S. Y.; Rubner, M. F.; Mayes, A. M. *Langmuir* **2002**, 18, 9600.
- Riegler, H.; Essler, F. *Langmuir* **2002**, 18, 6694.
- Chialvo, A. A.; Cummings, P. T.; Simonson, J. M.; Mesmer, R. E. *J. Chem. Phys.* **1999**, 110, 1064.
- Chialvo, A. A.; Simonson, J. M. *J. Phys. Chem. B* **2005**, 109, 23031.
- Messina, R.; Holm, C.; Kremer, K. *J. Polym. Sci., Part B: Polym. Phys.* **2004**, 42, 3557.
- Nandi, N.; Bagchi, B. *J. Phys. Chem. B* **1997**, 101, 10954.
- Messina, R. *J. Chem. Phys.* **2006**, 124, 014705.
- Messina, R. *Eur. Phys. J. E* **2007**, 22, 325.
- Panchagnula, V.; Jeon, J.; Dobrynin, A. V. *Phys. Rev. Lett.* **2004**, 93, 037801.
- Panchagnula, V.; Jeon, J.; Rusling, J. F.; Dobrynin, A. V. *Langmuir* **2005**, 21, 1118.
- Patel, P. A.; Jeon, J.; Mather, P. T.; Dobrynin, A. V. *Langmuir* **2005**, 21, 6113.
- Patel, P. A.; Jeon, J.; Mather, P. T.; Dobrynin, A. V. *Langmuir* **2006**, 22, 9994.
- Carrillo, J. M. Y.; Dobrynin, A. V. *Langmuir* **2007**, 23, 2472.
- Jeon, J.; Panchagnula, V.; Pan, J.; Dobrynin, A. V. *Langmuir* **2006**, 22, 4629.
- Terao, T. *Colloids Surf., A* **2006**, 273, 141.
- Terao, T. *Phys. Rev. E* **2002**, 66, 046707.
- Terao, T.; Nakayama, T. *Phys. Rev. E* **2002**, 65, 021405.
- Patra, C. N.; Chang, R.; Yethiraj, A. *J. Phys. Chem. B* **2004**, 108, 9126.
- Reddy, G.; Chang, R. W.; Yethiraj, A. *J. Chem. Theory Comput.* **2006**, 2, 630.
- Stevens, M. J.; Kremer, K. *J. Chem. Phys.* **1995**, 103, 1669.
- Weeks, J. D.; Chandler, D.; Andersen, H. C. *J. Chem. Phys.* **1971**, 54, 5237.
- Arnold, A.; de Joannis, J.; Holm, C. *J. Chem. Phys.* **2002**, 117, 2496.
- de Joannis, J.; Arnold, A.; Holm, C. *J. Chem. Phys.* **2002**, 117, 2503.
- de Joannis, J. Personal communication via e-mail on May 2003.
- Brodka, A. *Chem. Phys. Lett.* **2005**, 410, 446.
- Brodka, A., Personal communication via e-mail, March 29, 2006.
- Yeh, I.-C.; Berkowitz, M. L. *J. Chem. Phys.* **1999**, 111, 3155.
- Berendsen, H. J. C.; Grigera, J. R.; Straatsma, T. P. *J. Phys. Chem.* **1987**, 91, 6269.
- Aqvist, J. *J. Phys. Chem.* **1990**, 94, 8021.
- Smith, D. E.; Dang, L. X. *J. Chem. Phys.* **1994**, 100, 3557.
- van Veggel, F.; Reinhoudt, D. N. *Chem. Eur. J.* **1999**, 5, 90.
- Striolo, A.; Gubbins, K. E.; Chialvo, A. A.; Cummings, P. T. *Mol. Phys.* **2004**, 102, 243.
- Wang, B.; Kral, P. *Small* **2007**, 3, 580.
- Tasis, D.; Tagmatarchis, N.; Bianco, A.; Prato, M. *Chem. Rev.* **2006**, 106, 1105.
- Martyna, G. J.; Tuckerman, M. E.; Tobias, D. J.; Klein, M. L. *Mol. Phys.* **1996**, 87, 1117.
- Cheng, A. L.; Merz, K. M. *J. Phys. Chem.* **1996**, 100, 1927.
- Palmer, B. J. *J. Comput. Phys.* **1993**, 104, 470.
- Ryckaert, J. P.; Ciccotti, G.; Berendsen, H. J. C. *J. Comput. Phys.* **1977**, 23, 327.
- Andersen, H. C. *J. Comput. Physics* **1983**, 52, 24.
- Chialvo, A. A.; Cummings, P. T.; Cochran, H. D.; Simonson, J. M.; Mesmer, R. E. *J. Chem. Phys.* **1995**, 103, 9379.
- Chialvo, A. A.; Cummings, P. T.; Simonson, J. M.; Mesmer, R. E. *J. Chem. Phys.* **1996**, 105, 9248.
- Martinez, J. M.; Martinez, L. *J. Comput. Chem.* **2003**, 24, 819.
- Lue, L.; Evans, D. J. *Phys. Rev. E* **2000**, 62, 4764.
- Smith, W.; Forester, T. R. *Comput. Phys. Commun.* **1994**, 79, 52.
- Smith, W. *Comput. Phys. Commun.* **1992**, 67, 392.
- von Seggern, D. *Standard Curves and Surfaces*; CRC Press: Boca Raton, 1993.
- Jackson, J. D. *Classical Electrodynamics* 2nd ed.; John Wiley & Sons: New York, 1975.
- Jimenez-Angeles, F.; Lozada-Cassou, M. *J. Phys. Chem. B* **2004**, 108, 7286.
- Ravindran, S.; Wu, J. Z. *Langmuir* **2004**, 20, 7333.
- Messina, R.; Holm, C.; Kremer, K. *Langmuir* **2003**, 19, 4473.
- Paper 288b in the session on Fundamentals of Interfacial Phenomena at the 2008 Annual AIChE Meeting, Philadelphia, Nov. 18, 2008. Manuscript in preparation.